SPARC-BD-03/007
8 November 2003

SPARC INJECTOR WORKING POINT OPTIMIZATION

M.E. Biagini, M. Boscolo, M. Ferrario, V. Fusco, M. Migliorati, C. Vaccarezza, *(INFN/LNF),* L. Giannessi, L. Mezi, M. Quattromini, C. Ronsivalle *(ENEA/FIS),* S. Reiche, J. B. Rosenzweig *(UCLA)*

Abstract

Detailed analysis of the SPARC-FEL operation including different types errors in the undulator show that the previous set of beam parameters ($I \approx 85$ A , slice emittance $\epsilon_n \approx 1$ μm, with Q = 1 nC , pulse length of 11.7 psec and laser spot radius of 1 mm) does not leave a significant margin of contingency to ensure full saturation and testing of harmonic generation in the space of 14.5 m that has been allocated for the undulator. A more safe set of parameters requires a beam having 100 A in 50% of the slices with a slice emittance ≤ 1 μm . A new optimization and start to end simulations are reported in this note aiming to reduce the FEL saturation length to a more convenient level for fitting in the experimental hall.

1 INTRODUCTION

Detailed analysis of the SPARC-FEL operation including different types of errors in the undulator [1,2] show that the previous set of SPARC beam parameters [3] ($I \approx 85$ A , slice emittance $\varepsilon_n \approx 1$ μm, with Q = 1 nC , pulse length of 11.7 psec and laser spot radius of 1 mm) does not leave a significant margin of contingency to ensure full saturation and testing of harmonic generation in the space of 14.5m that has been allocated for the undulator. An analysis of the working point optimization for the SPARC FEL has been discussed in [1], where it has been pointed out that a viable solution to reduce the FEL saturation length to a more convenient level (i.e. fitting in the experimental hall) consists in a reduction of the period length and an increase of the beam current.

The optimization procedure has been obtained by keeping constant the electron beam energy of 150 MeV, the resonant wavelength $\lambda_r \cong 500$ nm and the external focusing strength (average betatron function $\beta_{avg} \cong 1.5$m). Concerning the problem of the external focusing it must be noted that a previous analysis of a low beta SPARC undulator configuration [4] has pointed out only marginal benefits consisting in a reduction of the saturation length of about 2m, accompanied by a significant reduction of the alignment tolerances for the beam/undulator systems, that easily thwart the advantages in terms of gain length shortening. The SPARC FEL will indeed operate with an uncompressed beam with relatively low current which should be characterized by a the state of the art design emittance. For this reason at the nominal $\beta_{avg} \cong 1.5$m the predicted electron beam average cross section amounts to ≈ 70 μm, a factor 8-10 times smaller than the transverse cross section of the amplified radiation (See Fig. 1). This is a clear sign of the fact that the FEL is dominated by diffraction effects.

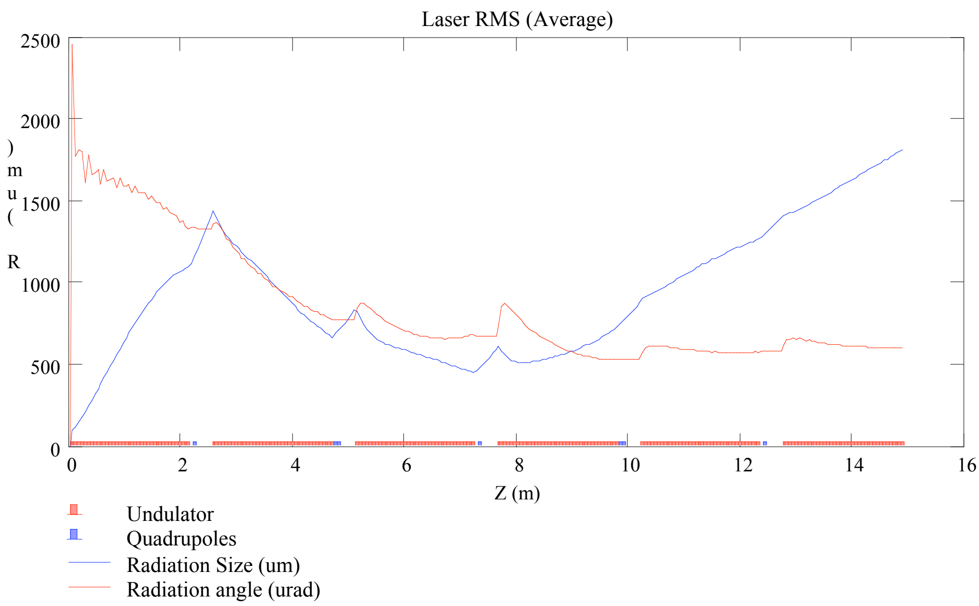

Fig. 1 – Radiation size (blue line) and radiation angle (red line) along the SPARC undulator. The electron beam size at the undulator entrance is supposed to be 50 μm.

At low energy, and with uncompressed photoinjector sources, it is indeed a general rule that diffraction plays an important role in the performances of a SASE FEL. In a diffraction dominated FEL regime the gain length L_g scaling law [5] is the following:

$$L_g \cong L_{1D}\left[1 + 0.45\left(\frac{L_{1D}}{Z_R}\right)^{0.57} + \ldots\right]. \tag{1}$$

where L_{1D} is the gain length as computed from the FEL 1D model.

$$L_{1D} = \frac{\lambda_u}{4\pi\rho\sqrt{3}}$$

The parameter ρ appearing in (2) is the Pierce parameter defined by

$$\rho = \frac{1}{4\pi\gamma}\left[2\pi^2 \frac{I}{I_{Alf}} \frac{\left(K\lambda_u f_B(K)\right)^2}{\Sigma_E}\right]^{\frac{1}{3}}$$

where $\Sigma_E = 2\pi\beta_{avg}\frac{\varepsilon_n}{\gamma}$ is the average electron beam cross section, with ε_n the normalized rms emittance, where

$$f_B(\xi) = J_0(\xi) - J_1(\xi), \qquad \text{and where} \quad \xi = \frac{1}{4}\frac{K^2}{1+\frac{K^2}{2}}$$

The Rayleigh range of the emitted coherent radiation of wavelength λ_r is written for a round beam of constant size σ_x as

$$Z_R = \frac{4\pi\sigma_x^2}{\lambda_r} = \frac{4\pi\beta_{avg}\varepsilon_n}{\lambda_r\gamma}. \qquad (2)$$

The scaling of the gain length with the Twiss function β_{avg} is the following

$$L_g \propto \beta_{avg}^{\frac{1}{3}}\left(1 + r\beta_{avg}^{-0.57\frac{2}{3}} + \ldots\right)$$

where *r* is a scaling constant depending on the other configuration parameters. A reduction of the beta coefficient increases the parameter ρ thus reducing the 1D gain length L_{1D}, but reduces the reference Rayleigh range and in conditions of strong diffraction it may even lead to an increase of the 3D gain length L_g. At $\beta_{avg} \approx 1.5$m the SPARC working point is still far from these conditions, but the dependence of the gain length from the focusing is weak; a reduction of beta of a factor 3 provides only $\approx 20\%$ of undulator length reduction [4].

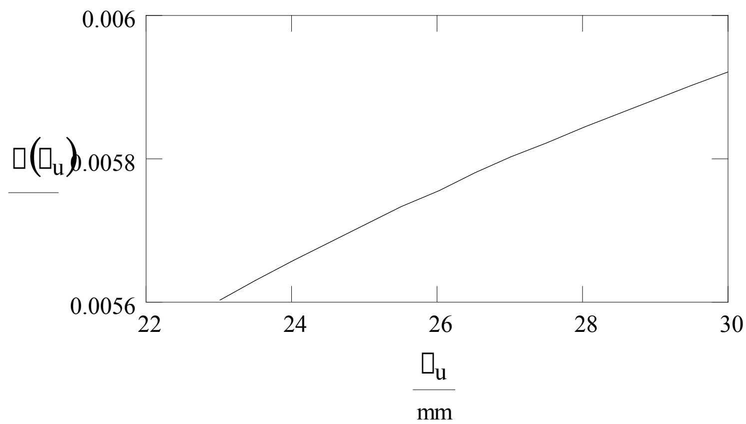

Fig. 2 – Pierce parameter as a function of the undulator period

The practical implementation of such a low beta optics requires a completely new undulator design that would be less compatible with future plans of operation at higher energy/lower wavelengths and would require much more stringent tolerances for transverse beam injection/alignment. In fig. 2 it is shown the behavior of the Pierce parameter vs the undulator period assuming the beam SPARC configuration of ref. [3].
The above plot has been obtained by keeping constant external focusing, with $\beta_{avg} \approx 1.5$m and setting the operation wavelength at 500 nm. The shortening of the period reduces the Pierce parameter, but this dependence, as it is evident from the figure, is very weak. For this reason, maintaining constant the focusing (β_{avg}) and the operation wavelength, implies that we are moving in the FEL parameter space, on a surface where the diffraction effects are maintained constant. The saturation length is then proportional to the 1D saturation length which is almost linearly proportional to the period length. The requested condition to keep the radiation wavelength fixed while reducing the period length, implies that we have to increase correspondently the undulator strength K according to

$$K = \sqrt{2\left(2\gamma^2 \frac{\lambda_0}{\lambda_u} - 1\right)}$$

and the period length optimization becomes a compromise between the availability of high field magnetic materials and choice of the minimum undulator gap compatible with the beam transport. The conclusions of ref. [1] suggested to reduce the design period length from 3 cm to 2.8cm and eventually to increase the peak current. This possibility was explored in more detail by reconsidering the working point for the injector in ref[5]. A safe SPARC configuration requires a beam having 100 A in at least 50% of the slices with a slice emittance $\leq$1 mm mrad, as discussed in paragraph 4. Simple scaling laws [6] allows us to change the beam quality according to the user's requirements without any modification of the beam line, as reminded hereafter.

The beam dynamics in a high brightness photoinjector can be conveniently described by the following rms envelope equation:

$$\sigma_x'' + \frac{(\beta\gamma)'}{\beta\gamma}\sigma_x' + k_x\sigma_x - \frac{2Ig(A)}{I_o(\beta\gamma)^3\sigma_x} = 0 \tag{4}$$

where $k_x = -\frac{F_{ext}}{\beta^2\gamma m_e c^2 \sigma_x}$ is the focusing strength for all linear static externally applied forces F_{ext}, and I_o = 17 kA is the Alfven current. A convenient scaling of the bunch parameters that does not require change in the external focusing and accelerating fields, i.e. that let the beam line untouched, results from the condition that the defocusing space charge wave number

$$k_{sc} = \frac{2Ig(A)}{I_o(\beta\gamma)^3\sigma_x^2} \propto \frac{Q}{\sigma_z\sigma_x^2}g(A) \tag{5}$$

remains constant which implies that peak the beam density and distribution shape $g(A)$, where $A = \frac{\sigma_x}{\sigma_z}$, must be kept constant . This condition can be fulfilled or quasi-fulfilled by four different approaches:

1) by keeping constant the aspect ratio $A = \frac{\sigma_x}{\sigma_z}$ so that $\sigma_x \propto \sigma_z \Rightarrow Q \propto \sigma_z^3 \Rightarrow I \propto \sigma_z^2$

2) by keeping constant the bunch length: $\sigma_z = const. \Rightarrow \sigma_x \propto Q^{1/2} \Rightarrow I \propto Q$

3) by keeping constant the bunch charge: $Q = const. \Rightarrow \sigma_x \propto \sigma_z^{-1/2} \Rightarrow I \propto \sigma_z^{-1}$

4) by increasing the bunch transverse dimension and the current with $\sigma_x \propto \left(\frac{Q}{\sigma_z}\right)^{1/2}$

In the next paragraph we discuss the choice of the new injector working point as a results of an extensive numerical analysis based on the previous scaling laws.

2 OPTIMIZED WORKING POINT

Being the SPARC injector the first one driving a saturating FEL without the use of a compressor scheme the FEL demand about the beam current means that we have to move towards the limits of the state of art for pulse charge and pulse shape. In order to reach the goal with a good level of confidence we explored a range of parameters that are not far from the best state-of-art performances. At present the best experimental results [8] give for a flat pulse with a FWHM=9 psec an emittance of 1.2 mm-mrad at Q=1 nC and an emittance of 1.5 μm at Q=1.2 nC, see Fig. 3. Keeping in mind these data we exploited a region of charge between 1-1.2 nC and a region of pulse length of 9-10 psec (FWHM). A detailed investigation of this range of parameters was done using PARMELA code.

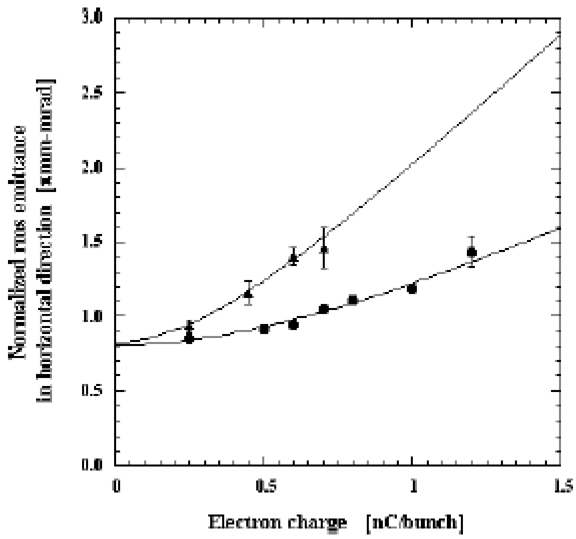

Fig. 3 Measured normalized emittance versus bunch charge for two temporal pulse distribution: gaussian (triangle) and square (dot) pulse shapes at pulse length of 9 psec FWHM

TAB. 1. Explored range of parameters

Q(nC)	**τ(psec) FWHM**	**Laser spot radius (mm)**
1	11.7	1
1	10	1.08
1.1	10	1.13
1.2	10	1.2
1	9	1.14
1.1	9	1.2

Starting from the parameters optimised for the working point at 85 A, the best performance with increasing launched current was obtained by means of the scaling approach 4) discussed in the previous paragraph. This condition requires the increase of the laser spot radius according with the table 1. In all cases a thermal emittance linearly increasing with the radius and equal to 0.3 μm for 1 mm of radius and a rise time of 1 psec were assumed.

The results of this study are summarized in Tab. 2 where the configuration that meets the requirement with the minimum emittance has been evidenced. It corresponds to a working point with 1.1 nC and a pulse length of 10 psec. In all cases a slice length of about 300μm has been considered.

TAB. 2. summary of PARMELA results for the 100 A in 50% beam working point

Q (nC)	τ (psec) FWHM*	Beam fraction with I ≥ 100 A	ε_n (μm)	Total rms energy spread	Max. slice rms energy spread**
1	11.7	0% (max. slice current ≈92 A) (average bunch current ≈86 A)	0.6	0.002	0.0005
1	10	23% (max. slice current ≈102 A) (average bunch current ≈94 A)	0.67	0.00162	0.0005
1.1	**10**	**54% (max. slice current ≈110 A) (average bunch current ≈102 A)**	**0.75**	0.00165	0.00052
1.2	10	60% (max. slice current ≈120 A) (average bunch current ≈110 A)	0.81	0.00166	0.00054
1	9	50% (max. slice current ≈110 A) (average bunch current ≈101 A)	0.8	0.00167	0.00042
1.1	9	58% (max. slice current ≈120 A) (average bunch current ≈110 A)	0.86	0.00167	0.00043

** rise time=1 psec, ** 85% of the particles*

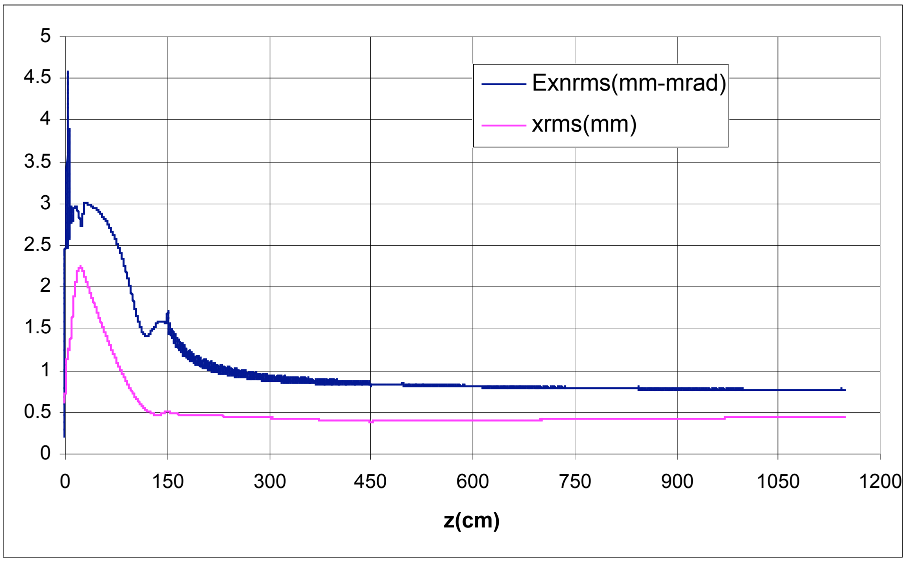

Fig. 3 - PARMELA computed RMS norm. Emittance and RMS horizontal envelope vs z from gun to the linac output for Q=1.1 nC, τ=10 psec, εth=0.34 mm mrad, laser spot radius=1.13 mm

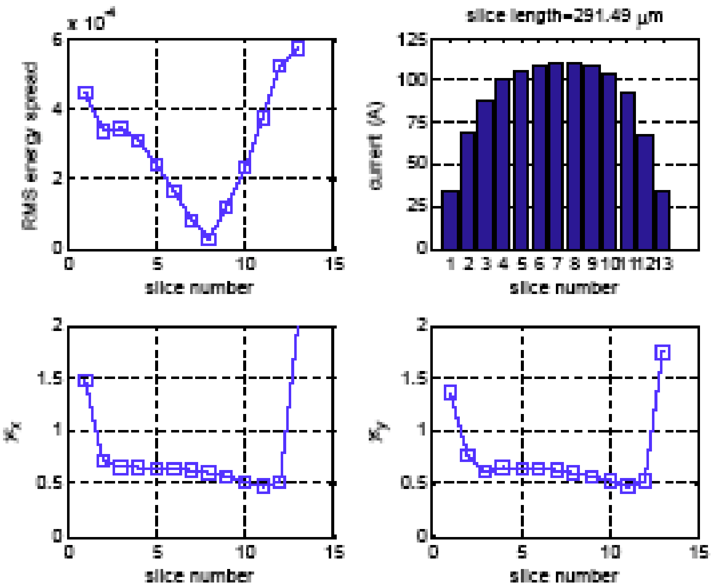

Fig. 4 - Computed slice parameters for Q=1.1 nC, τ=10 psec

One can observe from the Tab. 2 that it is not convenient to work with 9 psec of pulse length. This is due essentially to the fact that the higher aspect ratio increases the debunching longitudinal forces [3]. A pulse length of 10 psec allows to reach the SPARC-FEL goal without increasing the charge over the limits of the state-of-art.

In Fig. 3 the rms norm. emittance and the rms envelope in function of z from the gun to the linac output as computed by PARMELA are shown for the increased current working point. One can see that with the assumed scaling law the same parameters found for the working point at lower current (ϕgun=33°,Bgun= 2.73 Kgauss, B(TW section 1)=750 gauss, E(TW section 1)=25MV/m, E(TW section 2)=12.5MV/m, E(TW section 3)=12.5MV/m) preserve the emittance compensation scheme.

The plots of Fig. 4 refer to the slice analysis for this case: 85% of the particles are in slices with an emittance smaller than 0.7 mm mrad, 54% has a current ≥100 A and 70% has a current ≥90 A.

3 TRANSFER LINE AND UNDULATOR MATCHING OPTICS

A detailed analysis of the transfer line and the matching conditions to the undulator optics has been exploited in ref. [9] and the main conclusions of ref. 9 will be summarized in the following of this section. Two triplets are used to match the optical functions of the Linac beam to the values desired at the undulator entrance. This solution, as opposed to a doublet and a triplet configuration which was also suitable, has been chosen in order to assure the most flexibility to the line. A 0.7 m drift is left free after the first triplet to allow for the installation of a RF deflector for bunch length measurements, performed on a flag installed in the drift after the second triplet. To save space each quadrupole is only 10 cm long.

Two cases have been studied at 155.3 MeV and 200 MeV, with correspondingly different values of the beam optical functions and emittance at the Linac end. In Table 3 the beam the main TL parameters are summarized.

In Fig. 5 the behaviour of β_x and β_y from the end of the linac (corresponding to z = 0 in the plot) to the undulator input is plotted. The peak horizontal beam size is in Fig. 6. The matching has been done including the focal effects of 6 undulator sections interleaved by small horizontally focusing quadrupoles. The effect of each undulator section on the beam has been simulated as a vertically focusing quadrupole. The magnetic layout and quadrupole strengths for the 155 MeV case are summarized in Tab. 4, for the TL and the first undulator section (repeated 6 times). In both cases, 155. and 200 MeV, the average β value in the undulator is between 1.5 and 2. m.

Table 3. – *TL characteristics*

Energy (MeV)	155. – 200.	**Max beam size (μ)**	430.
Length (m)	5.4	**Max β_x (m)**	120.
Number of 0.1 m quads	6	**Max β_y (m)**	75.
Max quad strength (m^{-2})	10.	**Min β_x (m)**	0.6
Max gradient (T/m)	10. – 13.	**Min β_y (m)**	0.2

Tab. 4

Element	L_{tot} (m) from Gun	Strength (m^{-2}) @ 155 MeV	G (T/m) @ 155 MeV	Strength (m^{-2}) @ 200 MeV	G (T/m) @ 200 MeV
Drift	12.	-	-	-	-
Q1	12.1	-11.4	-5.9	-11.	-7.4
Drift	12.25	-	-	-	-
Q2	12.35	15.	7.8	14.	9.4
Drift	12.5	-	-	-	-
Q3	12.6	-2.6	-1.4	-1.85	-1.2
Drift	15.55	-	-	-	-
Q4	15.65	-14.8	-7.7	-14.6	-9.7
Drift	15.8	-	-	-	-
Q5	15.9	18.3	9.5	14.	9.3
Drift	16.05	-	-	-	-
Q6	16.15	10.5	5.4	12.6	8.4
Drift	16.9	-	-	-	-

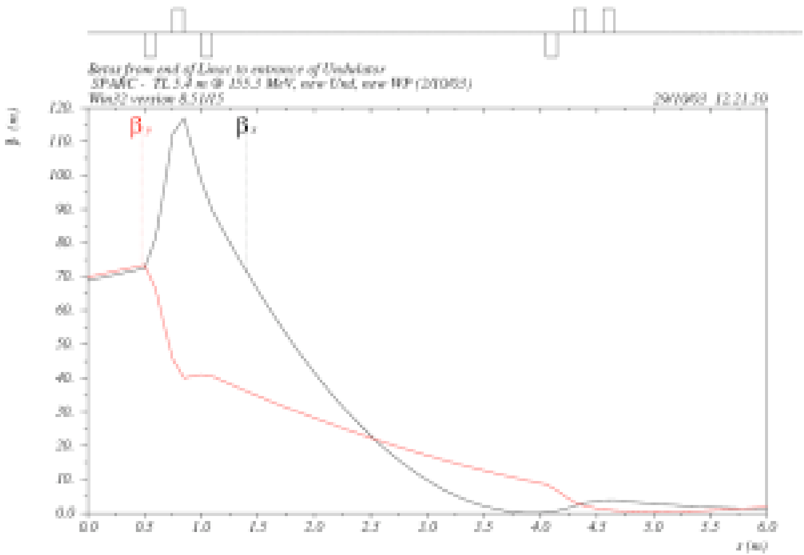

Fig. 5 *Optical functions in meters (black horizontal, red vertical), for the 155 MeV case, from the Linac output to the undulator input (z=0. corresponds to 11.5 m from the gun).*

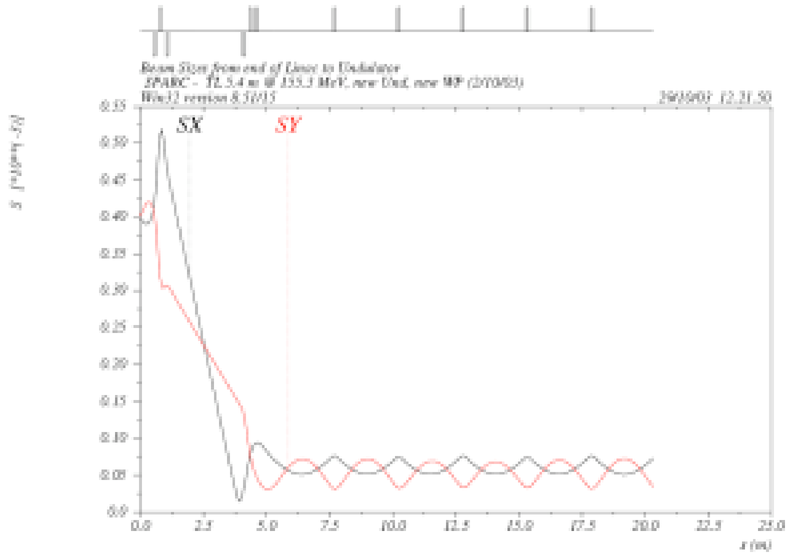

Fig. 6 *– Beam sizes in mm (black horizontal, red vertical) for the 155 MeV case, from the Linac output to the undulator output. The normalized beam emittance is 500 □m.*

The calculations of the matching parameters have been done by using the MAD code that does not take into account the space charge. In order to check the matching and to evaluate the effect of the space charge in the transfer line, the beam dynamics from the gun up to the undulator entrance for the nominal start-to-end configuration has been computed by using PARMELA code, switching on and off the space charge computation. In Fig. 7 the behaviour of the normalized rms emittance and rms envelope in the X and Y planes are shown as computed by PARMELA with the space charge included.

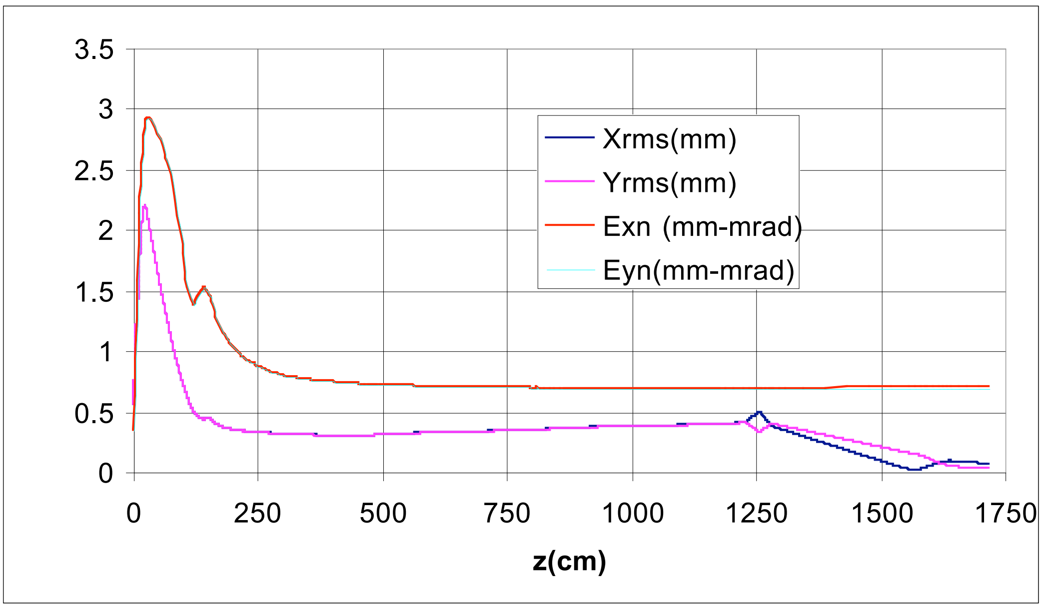

Fig. 7 *– Horizontal and vertical rms normalized emittances and envelopes from the gun to the undulator entrance*

Fig. 8 shows the beam phase space at the end of the TL with space charge on and off. One can see that when the space charge is off the agreement between the ideal values and the values given by the tracking is within 15%, while the mismatching increases when the space charge effect is taken into account: in particular the mismatching affects the Twiss parameters α_x and α_y.

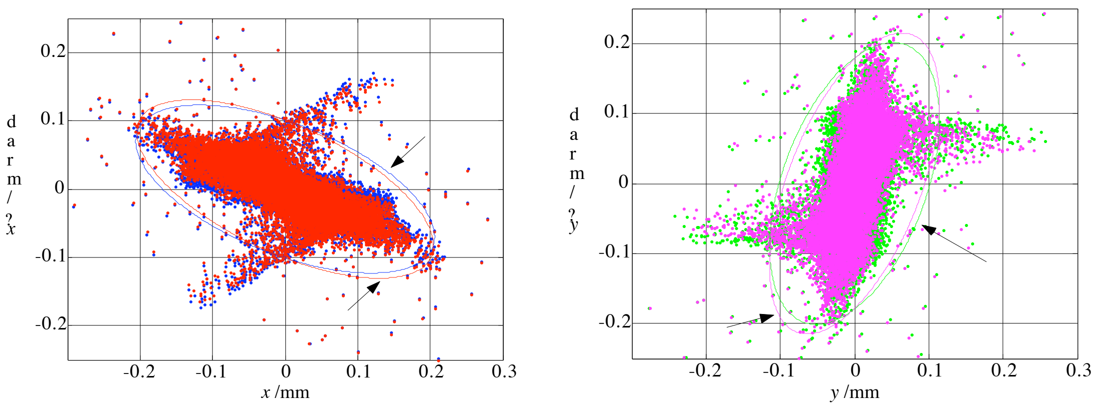

Fig 8 *– PARMELA computed X-X' and Y-Y' phase space at the end of the TL with the space charge on and off in the TL.*

These results refer to the whole beam, but the single longitudinal slices in general do not have exactly the same Twiss parameters of the whole bunch. So a slice analysis has been carried out in order to know the mismatching of the single slices of the bunch. In this analysis the slice length has been taken equal to about one cooperation length (~ 300 μm). The results are shown in Fig.9 where the x and y Twiss parameters and the relative mismatching parameters $M = 0.5(\beta_o\gamma - 2\alpha_o\alpha + \gamma_o\beta)$, ($\beta_o$,$\alpha_o$ and γ_o are the undulator matched parameters), are plotted in function of the slice number: one can see that 85% of the beam has a mismatching parameter lower than 1.2.

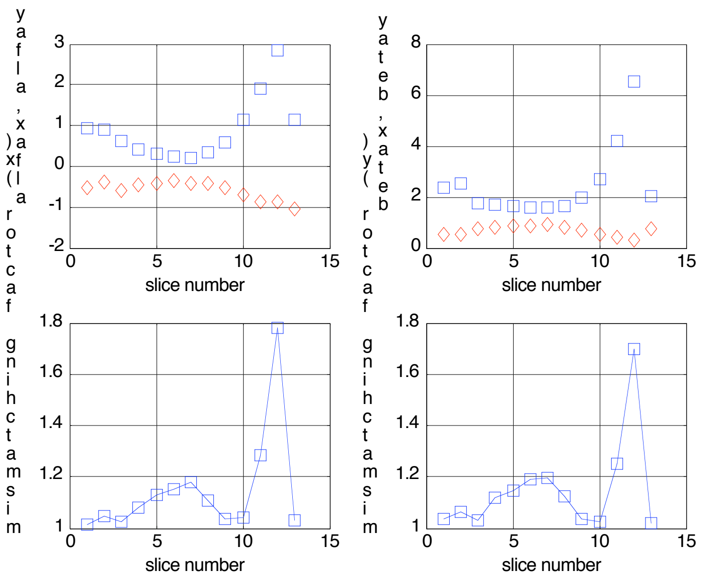

Fig10 *– Upper plots: Twiss parameters vs slice number. Lower plots: x and y mismatching parameter vs slice number*

4 FEL SIMULATIONS

The undulator parameter set used for the simulation are those of ref. [10] and are summarized in the following table

Period	2.8 cm
No of Periods/section	77 (+1 for phase matching)
No of Sections	6
K	2.145

FEL simulations based on average beam parameters have been analyzed in ref. [1] and [10]. In this note we summarize the results of a "Start to End" (StE) simulation obtained starting from the phase space generated by Parmela after transporting the beam through the injector, the linac, the transfer line, until the entrance of the undulator [11]. The beam phase spaces have been described in detail in the previous section (and in ref. [11]). As also anticipated in the previous section the beam optics in the undulator is realized taking advantage of the natural vertical focusing of the undulator itself. The matching conditions have been calculated by imposing that the vertical and horizontal beta functions are equal each other when averaged over one lattice period, and that the sum

$$\langle \Box_x \rangle^2 + \langle \Box_y \rangle^2$$

is minimized. The simulation has been performed using GENESIS 1.3 [12] in time dependent mode. In fig.11 the rms e-beam size is shown along the undulator.

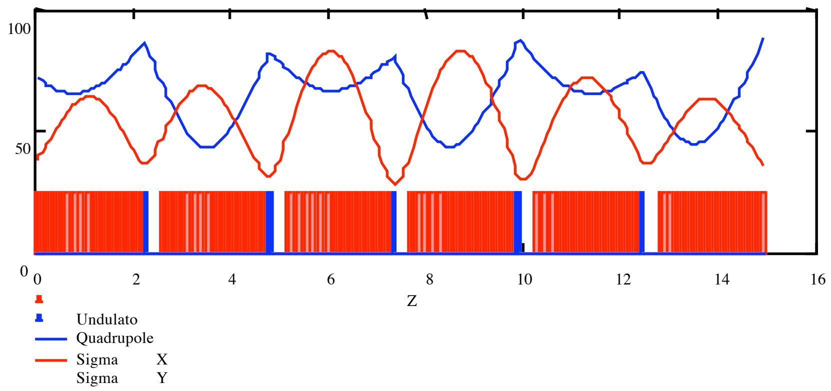

Fig.11 r.m.s. e-beam size vs z

The beam propagated by Parmela appears slightly mismatched with respect to the ideal case and the effect of this mismatching is the cause of the x-y asymmetry in the transverse rms. In fig. 12 the FEL power vs. z is shown. The saturation length is shorter than 9 m.
The radiation size and divergence that has been shown as an example in fig. 1 is one of the results of this simulation. The growth of the radiation rms width after 8 m is again a signature of occurring saturation. In fig. 13 it is shown the radiation power spectrum with the typical spiking of SASE FEL light.

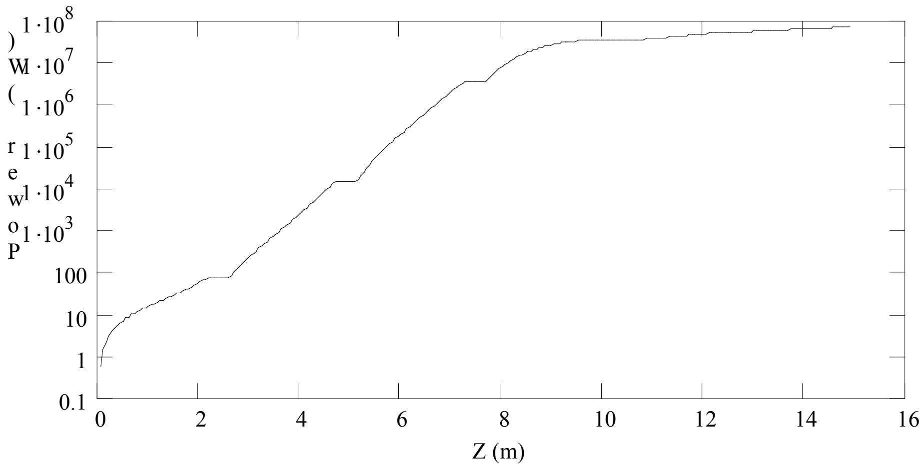

Fig. 12 Power vs. z for the SPARC FEL

Start to End simulations have been extremely precise in reproducing experimental data from other experiments and VISA is one of the main examples [see e.g. 13]. However we note that the StE simulation presented in this section has not been set up trying to reproduce a concluded experiment, but with the intention to anticipate the results of an experiment yet to be done. There is an important difference between these two situations. We have indeed to stress the fact that the electron beam has been "numerically" generated in ideal conditions, with an ideal laser pulse, from an ideal cathode and with all the parameters defining the configuration perfectly optimized. The contingency of more than 4 meters of undulator resulting from an analysis of fig. 12 gives a reasonable margin of operation, but starting from this ideal configuration an analysis of the FEL performances degradation due to the mismatch of different parameters will be the topic of forthcoming investigations.

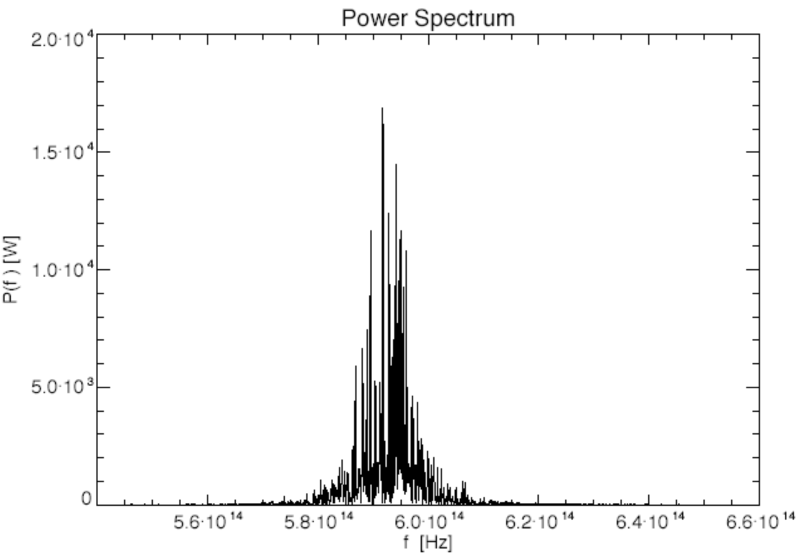

Fig 13. SPARC Power Spectrum

5 REFERENCES

[1] F.Ciocci, G. Dattoli, A. Doria, G.P. Gallerano, L. Giannessi, E. Giovenale, G. Messina, L. Mezi, P.L. Ottaviani1, L. Picardi, M. Quattromini, A. Renieri, C. Ronsivalle, "SPARC FEL Working Point And Undulator Configuration" **SPARC-FEL-03/001**

[2] L. Giannessi, "Simulazioni Genesis", Presented at the SPARC meeting of 10/04/2003 and available at http://www.afs.enea.it/sparc/riunioni/03_04_10

[3] D. Alesini et al., "Status of the Beam Dynamics Studies for the SPARC Project", **SPARC-BD-03/001**

[4] L.Giannessi, "Low Beta Undulator for SPARC", Presented at the SPARC meeting 30/04/2003 and available at http://www.afs.enea.it/sparc/riunioni/03_04_30/

[5] M. Xie, " Design optimization for an X-ray Free Electron Laser driven by SLAC linac", Proc. of PAC-95, Dallas 1995.
G. Dattoli, L. Giannessi, P. L. Ottaviani, and C. Ronsivalle , "Semi-analytical model of self-amplified spontaneous-emission free-electron lasers, including diffraction and pulse-propagation effects", Journal of Applied Physics Vol 95(6) pp. 3206-3210. March 15, 2004

[6] J. B. Rosenzweig et al., "Re-Examination of the working point for the SPARC injector and SASE FEL", **SPARC-BD-03/004**

[7] J.B. Rosenzweig and E. Colby, "Charge and Wavelength Scaling of RF Photoinjector Designs", *Advanced Accelerator Concepts* p. 724 (AIP Conf. Proc. 335, 1995).

[8] J. Yang et al. "Experimental studies of photocatode RF gun with laser pulse shaping", Proceedings of EPAC2002, Paris, p. 1828.

[9] L. Giannessi, L. Mezi, C. Ronsivalle, M. Biagini, M. Migliorati, G. Di Pirro, "SPARC Transfer Line", **SPARC-FEL-03/006**

[10] F. Ciocci, G. Dattoli, L. Giannessi, "SPARC Undulator parameter set", **SPARC-FEL-03/003**

[11] C. Ronsivalle, "New SPARC working point" Presented at the SPARC meeting 18.7.2003 and available at http://www.afs.enea.it/sparc/riunioni/03_07_18/

[12] S. Reiche, *Nucl. Instrum. & Meth.* **A429**, 243 (1999).
See also *http://corona.physics.ucla.edu/~reiche/*.

[13] S. Reiche, "Review of Application to SASE-FELs", in Proceedings of the ICFA Workshop "The Physics and Applications of High Brightness Electron Beams" Chia Lagune, Sardinia, July 1-6, 2002